Persistent properties of period doubling in directly modulated semiconductor lasers

Yao Huang Kao* and Hung Tser Lin
Department of Communication Engineering and Center of Telecommunication Research, National Chiao-Tung University, 1001 Ta Hsueh Road, Hsin-Chu, Taiwan 30050, Republic of China
(Received 11 January 1993)

In this paper the inherent properties of period-doubling behavior in deeply modulated laser diodes were investigated. The thresholds for the period doubling in terms of the controlling parameters were indicated. With the consideration of Langevin noise in the single-mode rate equations, it was indicated that the noise acted as a virtual Hopf precursor for the event of period doubling. The linewidth and frequency shifting of the noise bump were predicted by Floquet multipliers. Finally, a comparison of the noise bumps obtained from the simulated and analytic methods was also presented.

PACS number(s): 42.55.Px, 42.60.Fc, 02.50.−r, 05.45.+b

I. INTRODUCTION

Nonlinear dynamical behavior has been enthusiastically investigated in a wide variety of physical systems since the discovery of scaling constants in routes to chaos [1]. At least three scenarios of routes to chaos have been successfully applied to those systems. They are the Feigenbaum, intermittent, and quasiperiodic routes, and are related to the period-doubling, saddle-node, and Hopf bifurcations, respectively. As subjected to the nonlinear systems, the semiconductor lasers have also been intensively studied not only for theoretical interest, but also for practical purposes [2]. A solitary single-mode semiconductor laser cannot exhibit chaotic behavior because it is fully described by only two independent quantities: the photon density and carrier density. The adding of an additional degree of freedom, i.e., modulation, light injection, or delay feedback, is necessary for an allowance of the occurrence of chaotic instability. The aspect of the period-doubling route of a laser diode under direct-current modulation is the focus of this paper.

Strong current modulation in semiconductor laser diodes has recently received much attention, especially in the area of high-speed short-pulse generation and microwave analog fiber-optic transmission [3–18]. The output of photon density under such a circumstance exhibits a number of nonlinear phenomena, i.e., harmonic distortion, pulsation, bistability, quasiperiodic and period-doubling (PD) routes to chaos, etc. A set of nonlinear rate equations governing the interrelationship between carrier density and photon density have been successfully applied to forecast the relaxation oscillation and bistability [6,19]. The influences of nonlinear gain suppression factor, spontaneous emission factor, and Auger recombination factor in the rate equations upon the PD phenomenon have also been numerically examined [11,10–13]. The analytic method utilized for predicting the onset point of PD route has also been previously presented [14,15]. Despite great efforts, the important role of noise on the dynamics of the routes to chaos is not yet investigated in detail. The output of a cw diode laser actually exhibits a large-amplitude fluctuation with frequency around the relaxation oscillation frequency. These fluctuations arise from the quantum nature of spontaneous emission and cannot be eliminated in real diode lasers. In some sense the noise even plays a role of precursor for nonlinear instability. The noise spectra under the strong ac current modulation are investigated by numerical computations and compare with the AM noise theory [20]. It is demonstrated from the observable variable, such as photon density in our case, the noises play as a virtual Hopf precursor for the period doubling [21]. This study improves our understanding of the inherent properties of period doubling in semiconductor laser diodes.

The paper is organized as follows. The rate equations are introduced here in Sec. II with the consideration of Langevin noise. The algorithm of searching fixed points with the Newton-Raphson method in numerical computation is also presented. The explanations of virtual Hopf bifurcation by Floquet theory are presented in Sec. III. Concluding remarks are summarized in Sec. IV.

II. STOCHASTIC RATE EQUATIONS AND THEORETICAL BASIS

With the consideration of the nonlinear gain suppression, the single-mode rate equations for the photon density s and carrier density n can be written as [6,12]

$$\frac{dn}{dt}=\frac{I(t)}{eV}-\frac{n}{\tau_e}-A(1-\epsilon_{\rm nl}s)(n-n_0)s+F_n(t)/V\ , \quad (1)$$

$$\frac{ds}{dt}=\Gamma A(1-\epsilon_{\rm nl}s)(n-n_0)s-\frac{s}{\tau_p}+\frac{\Gamma\beta n}{\tau_e}+F_s(t)/V\ , \quad (2)$$

where e is the electron charge, V is the active volume, τ_e and τ_p are the respective electron and photon lifetimes, A is the gain constant, n_0 is the carrier density for transparency, Γ is the confinement factor, β is the spontaneous emission factor, and $\epsilon_{\rm nl}$ is the nonlinear gain suppression factor which can represent some mechanisms, including spatial hole burning, lateral carrier diffusion, spectral hole burning, and other nonlinearities [6]. The driving current containing dc and ac terms is expressed

as $I(t)=I_{dc}+I_{ac}\sin(2\pi ft)$ with driving frequency f. F_s and F_n are Langevin noise sources with zero means that respectively arise from spontaneous emission and from the discrete nature of the carrier generation and recombination.

The small-signal response of rate equations behavior is similar to that of a parallel underdamped oscillator [19]. The dynamical response can actually be characterized by two key parameters, the relaxation-oscillation frequency f_{RO} and damping factor η, which are given by

$$f_{RO}=\frac{1}{2\pi}\left[\frac{\Gamma A}{eV}\right]^{1/2}(I_{dc}-I_{th})^{1/2}\ , \tag{3}$$

$$\eta=(1/\tau_e+As_t+s_t\epsilon_{nl}/\tau_p+\beta\Gamma I_{th}/eVs_t)/4\pi f_{RO}\ , \tag{4}$$

where

$$I_{th}=eV[n_0+(\Gamma A\tau_p)^{-1}]/\tau_e\ ,$$

$$s_t=\Gamma\tau_p(I_{dc}-I_{th})/eV\ .$$

From the literature, the order of the damping factor is around 0.1 for the In-Ga-As-P laser. As regards to the wide-band Langevin noise, the output noise spectrum can be expressed as

$$S_a(f)=\frac{A_1[f^2+(2\eta f_{RO})^2]}{(f^2-f_{RO}^2)^2+(2\eta f_{RO}f)^2}\ , \tag{5}$$

where A_1 is the normalized constant as in Eq. (3.71) of Ref. [20]. The 3-dB bandwidth $\Delta f_{3\text{-dB}}$ in the frequency response can be easily predicted to be about $2\eta f_{RO}$.

As the modulation index is increased to a certain level, a sequence of dynamical bifurcations may be observed. The transitions related to the qualitative change of dynamic behaviors are generally able to be identified from the time evolution, phase portrait (s,n), and its Fourier spectra. Besides that, the Floquet theory is further employed here for examining the instability of optical intensity [14,21] so as to clarify the features of bifurcations. Equations (1) and (2) are rewritten for the sake of brevity as

$$\dot{X}=F(X;m)+\xi\ ,\quad X\in\mathbb{R}^N\ , \tag{6}$$

where $m=I_{ac}/I_{th}$ is the modulation index and ξ is Langevin noise with

$$\langle\xi(t)\rangle=0\ ,\quad \langle\xi_i(t)\xi_j(t+\tau)\rangle=\kappa_{ij}\delta(\tau)\ . \tag{7}$$

κ_{ij} is the noise strength. X^* is allowed to be a periodic solution of the noise-free system with $X^*(t+T)=X^*(t)$, where T is the period. For small deviation $\eta_d=X-X^*$, Eq. (6) can be linearized here about X^* so as to obtain

$$\dot{\eta}_d=[DF(X^*;m)]\eta_d+\xi\ , \tag{8}$$

where DF is the matrix of periodic functions with each term defined as

$$(DF)_{ij}=\left.\frac{\partial F_i}{\partial X_j}\right|_{X=X^*}\ . \tag{9}$$

Equation (8) is linear with periodic coefficients and is referred to as the Mathieu equation. The exact solution can be obtained using the Floquet theory. The external noise functions as a factor in kicking the system away from the limit cycle. The stationary solution X^* can be found here by using the Newton-Raphson algorithm and the Floquet multipliers μ can be obtained from the eigenvalues of the Jacobian $DF(X^*)$. In the observed case, the lowest period in the coefficients is also equal to T. The homogeneous solution φ_d in Eq. (8) then satisfies the property of

$$\varphi_d(t+T)=\mu\varphi_d(t)\ . \tag{10}$$

The stability of the stationary solution X^* can then be identified from the criterion with μ lying inside the unit circle, i.e., $|\mu|\le 1$. An instability occurs with μ crossing outside the unit circle. The period-doubling bifurcation occurs when a single μ is crossing the unit circle at -1 and the Hopf bifurcation occurs when a pair of μ and μ^* are moving across the unit circle. Moreover, the noise spectrum can be predicted from the situation of the μ value [21]. If the multiplier μ is expressed as

$$\mu=\exp(-\sigma T/2)\exp(i2\pi\Delta fT)=|\mu|\exp(i\theta)\ ,$$

then the bandwidth of the noise spectra is approximately equal to $\sigma/2\pi$ (Hz), the new peak position f_r is at $f_r=f-\Delta f$, and the peak height is equal to κ/σ. The noise spectrum can therefore be characterized from the site of a Floquet multiplier within the unit circle plane.

Accordingly, the finding of the stationary solution is the first task. To trace quickly the stable and unstable solutions, the Newton-Raphson algorithm is used here [22]. As in the periodically forced systems we can define a Poincaré section with point $X^i=(s(t),n(t))$ stroboscopically sampled at $t=2i\pi/\omega$, where i is an integer. The corresponding map $P_\Sigma(X^i)\to X^{i+1}$ is called a Poincaré map. X^* now becomes a fixed point of P_Σ with the relation of $P_\Sigma(X^*)=X^*$. The fixed point X^* can be calculated by iterating from an initial guess X^0 using the relation of

$$X^{i+1}=X^i-(DH(X^i))^{-1}H(X^i)\ , \tag{11}$$

where $H(X)\equiv X-P_\Sigma(X)$ and the superscript i indicates the interaction count as $P_\Sigma(X)$ is smooth. Knowing the fixed point, the onset point of instability and the type of bifurcation can be determined from the eigenvalue of the Jacobian $DF(X^*)$, i.e., Floquet multipliers. The results are detailed in the following sections.

The photo density and carrier density in Eqs. (1) and (2) are further normalized for numerical purposes by defining $P=s/s_0$ and $N=n/n_{th}$ with constant $s_0=\Gamma(\tau_p/\tau_e)n_{th}$ and the threshold carrier density $n_{th}=\tau_e I_{th}/eV$. The rate equations then become [12]

$$\frac{dN}{dt}=\frac{1}{\tau_e}\left[\frac{I(t)}{I_{th}}-N-\frac{N-\delta}{1-\delta}(1-\epsilon P)P\right]+F_n'\ , \tag{12}$$

$$\frac{dP}{dt}=\frac{1}{\tau_p}\left[\frac{N-\delta}{1-\delta}(1-\epsilon P)P-P+\beta N\right]+F_s'\ , \tag{13}$$

where

$$F_n' = F_n/(n_{\rm th}V) = \left[\frac{\left[\frac{I(t)}{I_{\rm th}} + N + \frac{N+\delta}{1-\delta}(1+\epsilon P)P\right]}{\tau_e \Delta t V n_{\rm th}}\right]^{1/2} X_n' ,$$

$$F_s' = F_s/(s_0 V) = \left[\frac{\left[\frac{N+\delta}{1-\delta}(1+\epsilon P)P + P + \beta N\right]}{\tau_p \Delta t V s_0}\right]^{1/2} X_n' ,$$

the constants $\delta = n_0/n_{\rm th}$ and the normalized gain suppression factor $\epsilon = \epsilon_{\rm nl} s_0$. The fourth-order Runge-Kutta algorithm with time step Δt and the fast-Fourier-transform (FFT) processor are employed here for finding the time evolution and frequency spectrum of the output photon density, from which the influences on the bistability and PD can be identified. These noise processes are assumed to be Gaussian random processes. In the Markovian assumptions, the autocorrelation and cross correlation functions of F_s and F_n are proportional to Dirac δ functions and can be expressed as [23]

$$\langle F_n(t)F_n(t')\rangle = V_n^2 \delta(t-t') , \tag{14a}$$

$$\langle F_s(t)F_s(t')\rangle = V_s^2 \delta(t-t') , \tag{14b}$$

$$\langle F_n(t)F_s(t')\rangle = \gamma_0 V_n V_s \delta(t-t') , \tag{14c}$$

where V_n and V_s are the respective variances of F_s and F_n, and γ_0 is the correlation coefficient. The variances can be expressed as follows:

$$V_n^2 = I/e + nV/\tau_e + A(1+\epsilon_{\rm nl})(n+n_0)sV , \tag{15a}$$

$$V_s^2 = sV/\tau_p + \Gamma A(1+\epsilon_{\rm nl}s)(n+n_0)sV + \Gamma A\beta nV/\tau_e , \tag{15b}$$

$$V_n V_s = -\{\Gamma A\beta nV/\tau_e + \Gamma A(1+\epsilon_{\rm nl}s)(n+n_0)sV\} . \tag{15c}$$

The correlation coefficient γ_0 approaches unity under the single-mode operation condition. The expressions for the variance apparently resemble rather closely the right-hand sides of the rate equations except that all terms become positive signs, because, physically, each term in the rate equations acts as a source of Gaussian noise. In numerical computation the stochastic functions F_s and F_n in any particular time interval Δt can be replaced by $F_n = V_n/\Delta t^{1/2} X_n$ and $F_s = V_s/\Delta t^{1/2} X_n$ with X_s and X_n denoting a Gaussian random variable of zero mean and unit variance. The noises X_n and X_s are generated within the computer. The time interval Δt is chosen to be $\Delta t = T/128$, where T is the period of the driving current. This ascertains that the noise spectrum is approximately white within $2f$ as of interest in the simulation. The required CPU time in a computer work station (HP-720) is approximately 16 ms for the simulation of one cycle. The calculation has been extended to 16 384 cycles and the first 100 cycles are discarded for removal of transients. The power spectra is calculated by using a fast Fourier transform with 32 768 points. The power spectra are further determined by averaging over 64 spectral components for the sake of improving the accuracy. This yields an error of less than approximately 1 dB.

III. NUMERICAL RESULTS

In the following, the thresholds in two specific cases with normalized gain suppression factor $\epsilon = 0$ and 0.01 are presented, which are closely related to the cases in Al-Ga-As and In-Ga-As-P semiconductor lasers [12]. For the sake of comparison, the typical values of the other parameters are chosen as $\tau_p = 6$ ps, $\tau_e = 3$ ns, $\beta = 5\times10^{-5}$, and $\delta = 0.692$ as identical to Refs. [10] and [12]. The normalized dc bias and ac modulated currents are defined as $I_b = I_{\rm dc}/I_{\rm th}$ and $m = I_{\rm ac}/I_{\rm th}$; m is also denoted as the modulation index. During the search for the transitions, the modulation frequency f and the modulation index m are varied with I_b at a fixed value. The relaxation-oscillation frequency $f_{\rm RO}$ under dc bias, approximately equal to 1.512 GHz in the observed case, can serve as a landmark in the parameter space during the search for the various transitions.

The possible transitions in the less-damped case with normalized gain suppression factor $\epsilon = 0$ [or $\eta \cong 0.0469$ from Eq. (4)] and without Langevin noise in Eqs. (12) and (13) are first presented to elucidate the rich variety of dynamical behaviors. The boundaries in m-f space for a typical case with dc bias current of $I_b = 1.5$ is shown in Fig. 1. The dynamical behaviors in output photon density include multiple and submultiple spiking, a period doubling route to chaos, and hysteresis, whereas the self-pulsation phenomenon is not observed. Their relevant transitions have been detailed in Ref. [24]. Generally speaking, at the modulation level beyond $m \simeq 0.5$, the

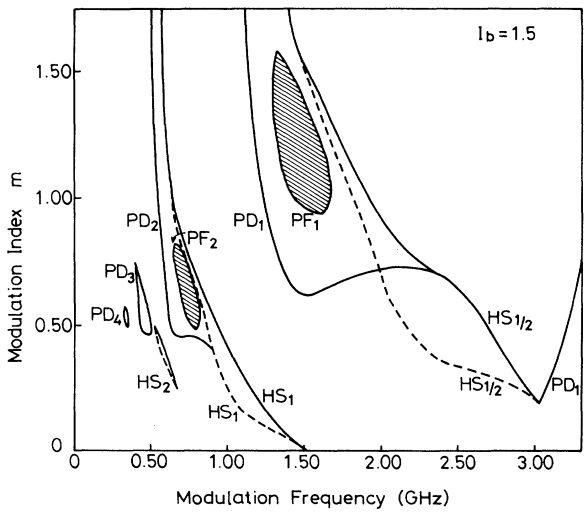

FIG. 1. Two-dimensional state diagram with modulation index and modulation frequency as controlled variables at fixed dc bias $I_b = 1.5$. Curve HS_m is the boundary of hysteresis jump of the mth spiking state; the dashed lines denote the downward jump. Curves PD_m and PF_m are the boundaries of period doubling and period four of the mth spiking state, respectively.

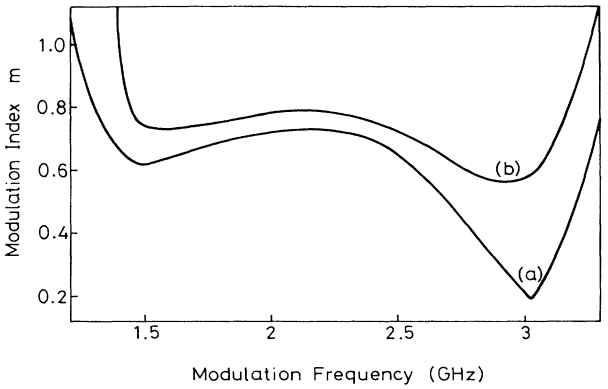

FIG. 2. U-shaped thresholds of period doubling with (*a*) $\epsilon=0.0$ and (*b*) $\epsilon=0.01$.

output contains multiple spikes for $f<f_{RO}$ and submultiple spikes for $f>f_{RO}$ and are closely related to the superharmonic and subharmonic resonance. The curve PD_1 is the threshold of period doubling with one spike state existing from f_{RO} to $2f_{RO}$. Thus, it seems to be the most expected transition in the real experiment because its threshold is lower than those at other regions [17]. The threshold of PD_1 basically reveals a U shape, as similar to that in the Toda oscillator [25], which possesses a potential well with an exponential form in its dynamical equation of motion. At the larger damped case with $\epsilon=0.01$ ($\eta\cong 0.0908$) the U-shaped threshold is lifted upward as in curve *b* of Fig. 2. It means that a more stronger ac current is required for attaining the period doubling in the higher damping case.

The influences of the Langevin noise on PD are further examined. First, the Floquet multipliers for both cases are calculated. The loci of the Floquet multiplier as a function of m at $I_b=1.5$ are shown in Figs. 3 and 4 with $\epsilon=0$ and 0.01, respectively, at three different pumping frequencies of $f=1.5$, 2, and 3 GHz. The radius in the low damped case ($\epsilon=0$) is obviously larger than that in the high damped case ($\epsilon=0.01$). The loci start from near $\theta\cong 0°$ for $f=1.5$ GHz, near $\theta\cong\pm 90°$ for $f=2$ GHz, and near $\theta\cong\pm 180°$ for $f=3$ GHz. Actually, we can deduce that the initial point starts approximately from $\theta=(j-1)\pi$ if the driving frequency is at $f\cong f_{RO}$; j is an integer. As m is increased, the multipliers rotate toward the negative real axis. The critical modulation index m_c defined with the complex pair merging at a critical value $\mu_c=-\exp(-\sigma T/2)$ on the negative axis is at $m_c\cong 0.615$, 0.715, and 0.04 for $f=1.5$, 2, and 3 GHz, respectively. The closer to $2f_{RO}$ the frequency is, the larger the radius $|\mu_c|$ is. Above the critical index m_c, the multiplier appears as two negative real pairs. One of the multipliers approaches -1 and causes period doubling. This kind of transition process is referred to as virtual Hopf bifurcation, because the complex conjugate pair lies initially very close to the unit circle, a situation that generally occurs just before the onset of a Hopf bifurcation. However, instead of exiting the unit circle, the multipliers move along the circle with radius $|\mu|=\exp(-\sigma T/2)$, until they meet on the negative real axis. m_p is the onset index for period doubling with one

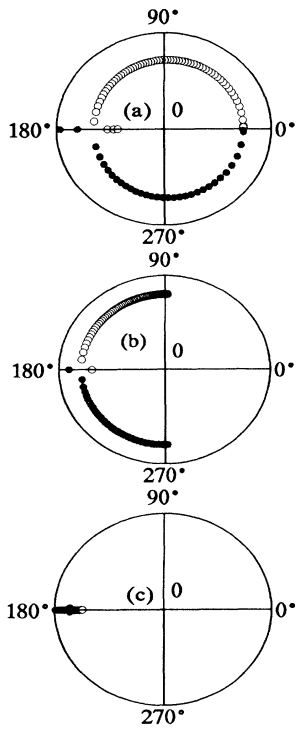

FIG. 3. The calculated loci of Floquet multipliers for $\epsilon=0$ and (a) $f=1.5$ GHz, (b) $f=2.0$ GHz, and (c) $f=3.0$ GHz.

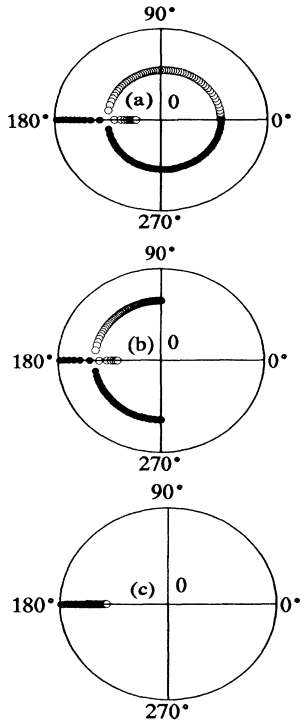

FIG. 4. The calculated loci of Floquet multipliers for $\epsilon=0.01$ and (a) $f=1.5$ GHz, (b) $f=2.0$ GHz, and (c) $f=3.0$ GHz.

TABLE I. Calculated values of m_c, m_p, and $|\mu|$.

	$\epsilon=0$			$\epsilon=0.01$		
f (GHz)	m_c	m_p	$\lvert\mu_c\rvert$	m_c	m_p	$\lvert\mu_c\rvert$
	0.615	0.64	0.6582	0.635	0.73	0.5036
	0.715	0.72	0.7929	0.715	0.77	0.6443
	0.04	0.28	0.8617	0.01	0.55	0.7503

of the Floquet multipliers μ just passing through the unit circle. For convenience, the calculated values m_c, m_p, and $|\mu_c|$ for both cases ($\epsilon=0$ and $\epsilon=0.01$) are listed in Table I.

The noise spectra can thus be predicted from the site of the multiplier within the unit circle. Figures 5 and 6 demonstrate the corresponding spectra for $\epsilon=0$ and 0.01. The peak frequencies are centered around the relaxation oscillation frequency f_{RO} without ac current as in Figs. 5(a) and 6(a). The linewidth of the bumps is easily determined by $\Delta f_{3\mathrm{dB}}=2\eta f_{\mathrm{RO}}$ ($\cong 142$ MHz in $\epsilon=0$ and 275 MHz in $\epsilon=0.01$). The bump shifts toward $f/2$ as m is increased. Except for the original bump, there are also a lot of bumps distributed among both sides of the subharmonic frequencies as in Figs. 5(b) and 6(b). This is the nature of the complex conjugates of Floquet multipliers. For $m \leq m_c$ the noise bump is confirmed to maintain the same width as that without modulation by comparing Figs. 5(a) and 5(b) or Figs. 6(a) and 6(b). Physically, the shiftiness of the bump is that, under the large excitation, the photon density can deplete more of the carrier density and thus requires more time to recover the carrier density. Consequently, the relaxation oscillation frequency is decreased. The frequency shift as a function of driving force m is shown in Fig. 7. The dotted points are obtained by noise spectra, the solid line is from the information of angle θ, and the broken line is fitted from the relation of $\Delta f=\Delta f_0+dm^2$ with $\Delta f_0=0.488$ GHz and constant $d=0.807$ GHz. Actually, Δf_0 is the initial frequency difference between the bump and the driving frequency, i.e., $\Delta f_0=f-f_{\mathrm{RO}}$. As for the constant d, it is an implicit function of the damping factor η. The less η is, the larger d is. It seems that the frequency shift is in good agreement with the dependence of m^2.

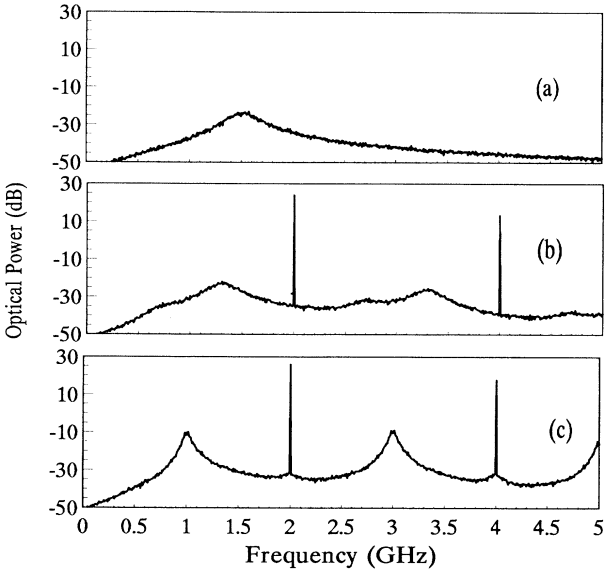

FIG. 6. The noise spectra at $\epsilon=0.01$, $f=2$ GHz, $I_b=1.5$ and (a) $m=0$, (b) $m=0.5$, and (c) $m=0.75$ before period doubling.

At the critical index with repeated multipliers, the spectra reveal only one bump with peak at $f/2$. Above the critical index, the repeated pair split into two negative real numbers and one of them approaches toward -1. In such a case, the shape of the bump shown in Fig. 6(c) becomes narrower and narrower, but with the maximum still fixed at $f/2$, as the excitation reaches closer

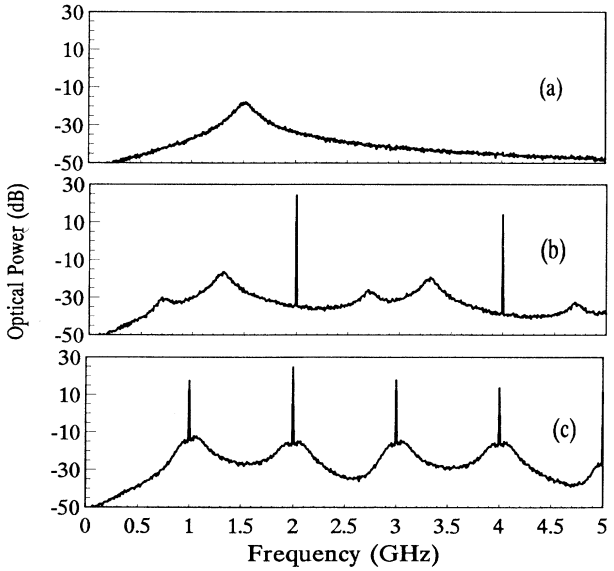

FIG. 5. The noise spectra at $\epsilon=0.0$, $f=2$ GHz, $I_b=1.5$ and (a) $m=0$, (b) $m=0.5$, and (c) $m=0.75$ after period doubling.

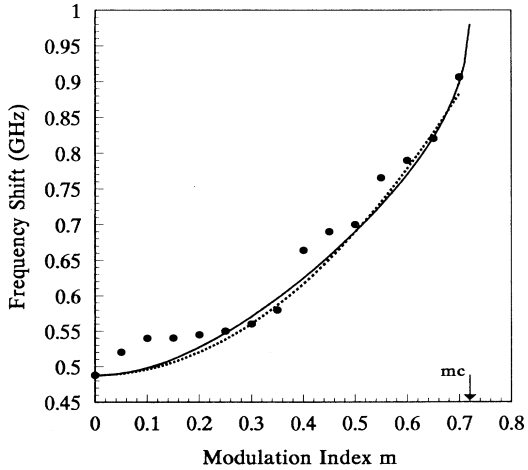

FIG. 7. The dependence of the peak shift of noise bump on modulation index for $\epsilon=0.01$. The broken line is calculated from the relation of frequency shift $\Delta f=\Delta f_0+dm^2$ with $\Delta f_0=0.488$ GHz and $d=0.807$ GHz. The dotted line is obtained by noise spectra. mc is the critical modulation index with complex multipliers merging together.

and closer to the onset point m_p of period doubling. The narrowed bump may cause a mistake in identifying the behavior of period doubling during the real experiment. As a matter of fact, the true spikes for PD do not extrude from the noise bump until $m \geq m_p$ as in Fig. 5(c). At the same time, the level of the noise bump around the $f/2$ is significantly suppressed. Note that, if the driving frequency is near the specific frequency $2f_{\mathrm{RO}}$, PD occurs easily with only a small amount of excitation because μ is close to the negative axis.

At last, some notes on the line shape of the noise bump are given. Two spectra formulas are proposed to evaluate the spectra before onset of period doubling. One is

$$S_a'(f)=\frac{A_1[f^2+(2\eta f_r)^2]}{(f^2-f_r^2)^2+(2\eta f_r f)^2}\ , \tag{16}$$

which is similar to Eq. (5) but with f_{RO} replaced by f_r. The other is the Lorentz linewidth as [21]

$$S_{\mathrm{Lo}}(f)=\frac{A_2}{\Delta\nu^2+(f-f_r)^2}\ , \tag{17}$$

where A_2 is the normalized constant, and $\Delta\nu$ is half of the bandwidth. The comparisons are illustrated in Fig. 8. With regard to the 3-dB bandwidth, both formulas give almost the same results, whereas the overall shape of the main bump is more favorable to that predicted from Eq. (16) (solid line). The constant width of the bump with $m \leq m_c$ is confirmed from Figs. 8(a) and 8(b) to be equal to that with $m=0$. The linewidth is narrowed and is proportional to the σ factor as the index is above m_c. This is evidenced in Fig. 8(c) with the fitted linewidth about 70 MHz for $\sigma T/2=0.106$ (i.e., $2\Delta\nu=\sigma/2\pi\cong 70$ MHz). Although the Lorentz shape cannot fit well to the whole bump, it is good for the 3/2 bump as predicted in Ref. [21].

IV. CONCLUSIONS

The noise effects on the period doubling of the current modulated semiconductor laser were extensively investigated in this article. Focus was on the most remarkable range with a U-shaped threshold in the frequency interval

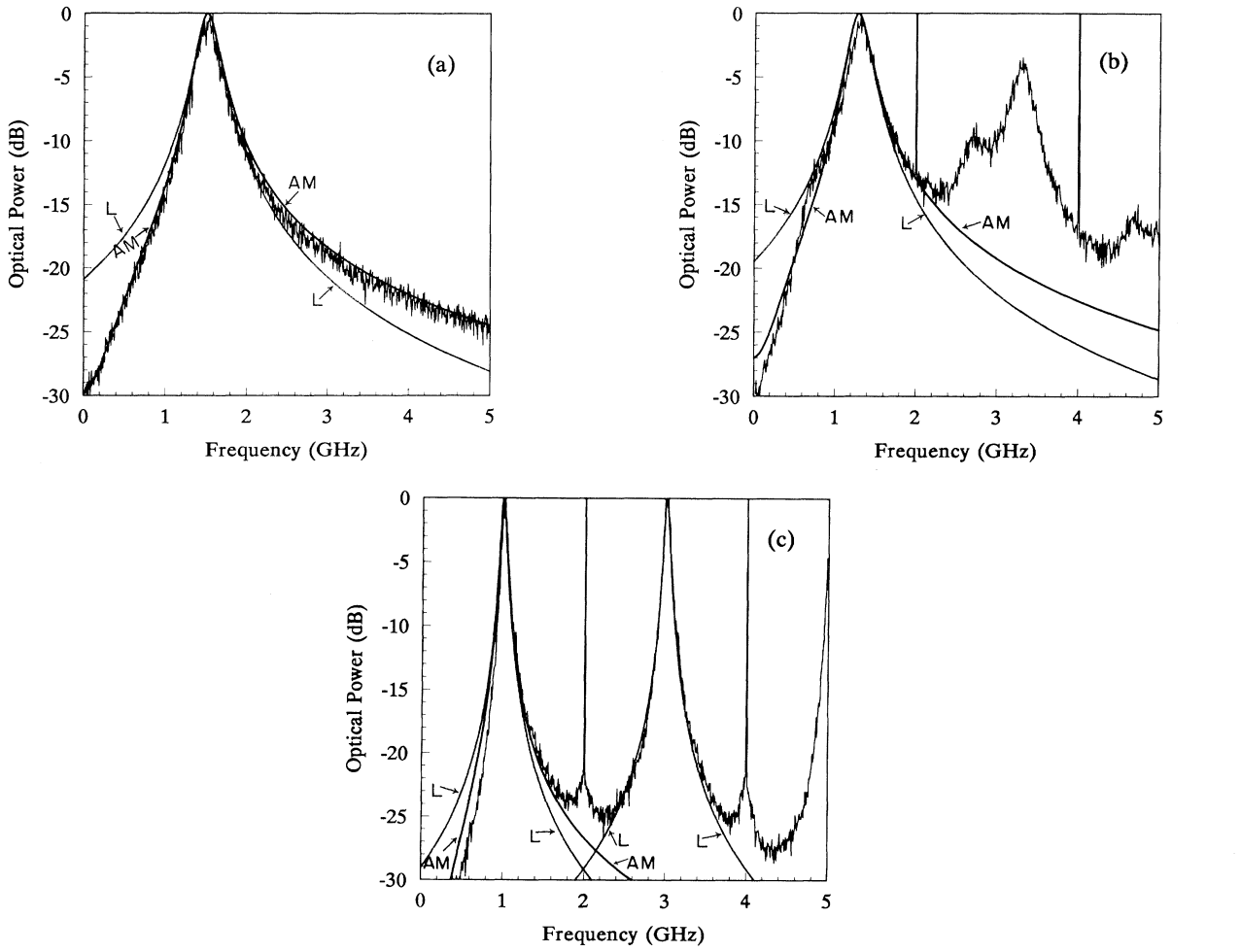

FIG. 8. The comparison of the calculated noise spectra with those from the Lorentz shape (curves labeled by L) and AM noise theory (curves labeled by AM) with $f=2$ GHz, $\epsilon=0.01$, and (a) $m=0$, $\sigma T/2=0.431$ ($2\Delta\nu\cong 274.5$ MHz), (b) $m=0.5$, $\sigma T/2=0.431$ ($2\Delta\nu\simeq 274.5$ MHz), and (c) $m=0.75$, $\sigma T/2=0.106$ ($2\Delta\nu\cong 70$ MHz).

between f_{RO} and $2f_{RO}$. Conceptually, the laser diodes could be taken as a current-controlled tunable amplifier with Langevin noise as a wide-band input signal. It was indicated that the inherent noise bump in the output spectrum played as the virtual Hopf precursor for the period doubling bifurcation. The behaviors of the noise bump were verified to follow the predictions from the Floquet multipliers. Once the initial relaxation frequency and damping factor were determined, the noise process up to period doubling could be clearly forecasted.

ACKNOWLEDGMENT

This study was supported by the National Science Council, Republic of China, under Contract No. NSC81-0404-E009-24.

*FAX: (886) 35-710116.

[1] J. P. Eckmann, Rev. Mod. Phys. **53**, 643 (1981).
[2] J. Sacher, D. Baums, P. Panknin, W. Elsasser, and E. O. Gobel, Phys. Rev. A **45**, 1893 (1992).
[3] W. Harth, Electron. Lett. **9**, 532 (1973).
[4] S. Tarucha and K. Otsuka, IEEE J. Quantum Electron. **QE-17**, 810 (1981).
[5] D. F. G. Gallagher, I. H. White, J. E. Carroll, and R. G. Plumb, IEEE J. Lightwave Technol. **LT-5**, 1391 (1987).
[6] R. S. Tucker and I. P. Kaminow, IEEE J. Lightwave Technol. **LT-2**, 385 (1984).
[7] C. H. Lee, T. H. Yoon, and S. Y. Shin, Appl. Phys. Lett. **46**, 95 (1985).
[8] Y. C. Chen, H. G. Winful, and J. M. Liu, Appl. Phys. Lett. **47**, 208 (1985).
[9] H. G. Winful, Y. C. Chen, and J. M. Liu, Appl. Phys. Lett. **48**, 616 (1986).
[10] M. Tang and S. Wang, Appl. Phys. Lett. **48**, 900 (1986).
[11] M. Tang and S. Wang, Appl. Phys. Lett. **50**, 1861 (1987).
[12] G. P. Agrawal, Appl. Phys. Lett. **49**, 1013 (1986).
[13] Y. Hori, H. Serizawa, and H. Sato, J. Opt. Soc. Am. B **5**, 1128 (1988).
[14] N. H. Jensen, P. L. Christiansen, and O. Skovgaard, IEEE Proc. **135**, 285 (1988).
[15] T. H. Yoon, C. H. Lee, and S. Y. Shin, IEEE J. Quantum Electron. **QE-25**, 1993 (1989).
[16] L. Chusseau, E. Hemery, and J. Lourtioz, Appl. Phys. Lett. **55**, 822 (1989).
[17] E. Hemery, L. Chusseau, and J. Lourtioz, IEEE J. Quantum Electron **QE-26**, 633 (1990).
[18] Y. H. Kao and H. T. Lin, Opt. Commun. **88**, 415 (1992).
[19] J. Katz, S. Margalit, C. Harder, D. Wilt, and A. Yariv, IEEE J. Quantum Electron. **QE-17**, 4 (1981).
[20] T. Okoshi and K. Kikuchi, *Coherent Optical Fiber Communications* (Kluwer Academic, Boston, 1988), Chap. 3, pp. 61–110.
[21] Frank Moss and P. V. E. McClintock, *Noise in Nonlinear Dynamical Systems* (Cambridge University Press, Cambridge, 1989), Vol. 2, Chap. 7, pp. 145–161.
[22] T. S. Parker and L. O. Chua, *Practical Algorithms for Chaotic Systems* (Springer-Verlag, New York, 1989).
[23] D. Marcuse, IEEE J. Quantum Electron. **QE-20**, 1139 (1984).
[24] Y. H. Kao, C. H. Tsai, and C. S. Wang, Rev. Sci. Instrum. **63**, 75 (1992).
[25] T. Kurz and W. Lauterborn, Phys. Rev. A **37**, 1029 (1988).